COPYRIGHT NOTICE

XIV International Conference on Computational Plasticity. Fundamentals and Applications
COMPLAS 2017
E. Oñate, D.R.J. Owen, D. Peric and M. Chiumenti (Eds)

PLASTIC DILATION RATE CHARACTERISTIC OF CONCRETE CONFINED WITH STEEL TUBE

BAMBANG PISCESA[*], MARIO M. ATTARD[*] AND ALI K. SAMANI[†]

[*] School of Civil Engineering and Environmental
University of New South Wales
Kensington, Sydney NSW 2051, Australia
e-mail: bambang.piscesa@unsw.edu.au and m.attard@unsw.edu.au

[†] School of Civil Engineering and Information Technology
Federation University
Ballarat, VIC 3350, Australia
email: a.khajehsamani@federation.edu.au

Keywords: Plastic dilation rate, concrete-filled-steel-tube, external confinement.

Abstract. The use of external confining devices to confine concrete has become widely used. One of the purposes is to gain additional concrete strength and ductility. Although there are many types of external confining devices, in this paper, the attention is limited to the use of the steel tube as an external confining device. One of the main objectives of this research is to study the plastic dilation rate behavior of concrete-filled-steel-tube (CFST) columns. The experimental data for the plastic dilation rate is extracted, and compared with the authors concrete plasticity model. In the authors' previous research, the calibration of the plastic dilation rate model was based on confined concrete tested under both active and passive confinement using FRP wraps. Since the behavior of the steel tube and the FRP materials are different, the author's plastic dilation rate model needs to be re-evaluated for CFST columns. Comparisons of the extracted experimental plastic dilation rates with the model prediction for CFST specimens with normal strength concrete show good agreement and requires no adjustment in the formulation. However, for a specimen with 80 MPa concrete, the proposed formulation shows slightly lower plastic dilation rates. More experimental data for CFST using high strength concretes is required for further investigation. For the sake of completeness, the overall response of two CFST specimens is also evaluated using an in-house three-dimensional non-linear finite element analysis (3D-NLFEA) using the author's proposed plasticity formulation for confined concrete.

1 INTRODUCTION

The use of external confining devices to confine concrete is widely used. The external confining device is defined as any material other than concrete (such as FRP or steel tube) which has a mechanism to provide a kinematic lateral restraint [1] for the confined material. One of the purposes is to gain additional concrete strength and ductility. The kinematic lateral restraint is related to the lateral modulus (E_L) of the external confining devices. The lateral

modulus (E_L) of the confining device can be computed by solving the compatibility equation between the external confining device and the concrete core. By using E_L, the effectiveness of the confinement can be measured. For an external confining device made of a material with a simple stress-strain relationship, such as FRP wrap, the lateral modulus E_L can be assumed to be constant throughout the loading. However, for a concrete-filled-steel-tube (CFST) the lateral modulus E_L keeps changing once the steel yields.

Recently, the authors proposed a constitutive plasticity model [2, 3] for confined concrete. In this model, the flow rule is a function of the plastic dilation rate of the confined concrete. The plastic dilation rate (β) was defined as the ratio of the lateral to axial plastic strains ($\beta = \varepsilon^{p}_{lat} / \varepsilon^{p}_{axial}$). The plastic dilation rate formulation itself is a function of the confining pressures of the concrete core and lateral modulus (E_L) of the external confining device. The proposed plastic dilation rate model was calibrated using the experimental data from both active and passive confinement. However, for the passive confinement, the calibration of the plastic dilation rate was solely based on the FRP confined concrete [2], and therefore, further validation of the proposed model with different types of the external confining devices needs to be carried out.

In this paper, the model of [2, 3] is validated for cases where the steel tube is used as the external confining device. The focus is to obtain the plastic dilation rate behavior of the concrete-filled-steel-tube (CFST). The steel tube material has a different behavior in comparison to FRP material. The FRP material has a linear elastic behavior up to failure and is considered an orthotropic material. Usually, the axial load carrying capacity of the FRP tube is sufficiently small and thus neglected in the analysis. In contrast, the steel tube material is considered as an isotropic material and obeys a J2 plasticity model with zero hardening modulus. When the CFST column is axially loaded, due to the higher elastic modulus in comparison with the concrete material, the steel tube yields first before the concrete core reaches its peak stress capacity. Further, at the state where the steel tube is yielding, the axial stress is much higher than the stress in the other directions which may complicate the measurement of the lateral modulus, as well as the confining pressures to the concrete core. Hence, investigating the plastic dilation rate characteristic for CFST is a challenge.

To maintain clarity in the discussion, the sections in this paper are organized by firstly presenting a short introduction showing the main objective of the paper followed by the study on the plastic dilation rate behavior for CFST. In the second section, previous studies on the plastic dilation rate behavior for FRP confined concrete and then the plastic dilation rate behavior for the CFST are discussed. It will be shown that despite the different constitutive behavior between the FRP confined concrete and CFST, the authors' plastic dilation rate formulation is sufficiently accurate and adaptable. In the third section, numerical modeling to investigate the performance of the authors' plasticity model is presented by using a three-dimensional non-linear finite element analysis (3D-NLFEA) developed by the authors [4]. Finally, conclusions are drawn, and some future research suggested.

2 PLASTIC DILATION RATE BEHAVIOR OF CFST

The plastic dilation rate from any experiment is evaluated by observing the changes of the plastic strain both in the lateral and axial direction. However, from the experiments, mostly, only the axial force, axial strain and circumferential strain are obtained. Hence, to get the plastic

dilation rate from the experiments, the raw data needs to be further processed. During the extraction process, some assumptions are made, and it is important to note that different assumptions may lead to a different value for the plastic dilation rate. The plastic dilation rate itself is highly sensitive to the increment of the selected data points from the experiment. The smaller the increment, the distortion of the plastic dilation rate becomes more pronounced. Due to this sensitivity, obtaining the data from available experiments in the literature requires a special filtering, unless, the experiments have complete data sets including the computed confining pressure and the axial stress within the concrete core.

To extract the confining pressure from the experiments, it is required computing the stress in the radial direction which is equal to the confining pressure of the concrete core. In the case of FRP confined concrete, because the FRP material is always elastic up to the fracturing point, the computation of the confining pressure is obtained by multiplying the lateral strain with the lateral modulus of the FRP confining device. Further, for FRP confined concrete, the axial stress in the FRP material can be neglected. These material assumptions simplify the data extraction for the plastic dilation rate. However, for an external confining devices with a yield point such as a steel-tube, computing the confining pressure must conform to the stress-strain relation of the J2 material. Generally, during the loading, initially before the steel starts to yield, the axial stress in the steel tube is higher than the stresses in other directions. Once the steel yields, the axial stress in the steel tube reduces and the stresses in other directions increase.

Before looking further at the plastic dilation rate behavior for CFST columns, it is important to understand the plastic dilation rate behavior for FRP confined concrete. Figure 1 shows the plastic dilation rate behavior for FRP confined concrete extracted from experiments. A method to extract the plastic dilation rate for FRP confined concrete is explained in [2]. The expression of the plastic dilation rate formulation at peak stress in [2] is written here as:

$$\beta = \beta_0 + \left(\beta_{\text{core}} - \beta_0\right)\tanh\left(a_4\left(\frac{f_{\text{r}}}{f_{\text{c}}^{'}}\right)^{b_4}\right) \tag{1}$$

in the above, β_0 is the uniaxial plastic dilation rate at the peak stress, β_{core} is the upper limit of the plastic core compaction, a_4 and b_4 are the calibrated parameters. Samani and Attard [5] suggested a value for β_0 of -2.5. The upper limit of the plastic core compaction (β_{core}) is calibrated with the experimental data for FRP confined concrete and is a function of both the confining pressure (f_{r}) and the lateral modulus (E_{L}) of the external confining devices. However, the value for β_{core} should not be less than the elastic Poisson's ratio of the external confining devices (μ_{Ext}). The expression for β_{core} is:

$$\beta_{\text{core}} = -0.5 + 0.0275\Phi \le -\mu_{\text{Ext}} \qquad \Phi = \sqrt{\frac{f_{\text{r}}}{f_{\text{c}}^{'}}\frac{E_{\text{L}}}{f_{\text{c}}^{'}}} \tag{2}$$

in the above, f_{c} is the uniaxial concrete compressive strength. In [2], the calibration of the parameters a_4 and b_4 uses a genetic optimization algorithm, and the expressions for both parameters are:

$$a_4 = 2.5 + 0.25\sqrt{\frac{E_{\text{L}}}{f_{\text{c}}^{'}}} \quad b_4 = 0.0915\sqrt{f_{\text{c}}}\exp\left[-0.0192\Phi\left\langle f_{\text{c}}^{'} - 73\right\rangle\right] \quad \Phi = \sqrt{\frac{f_{\text{r}}}{f_{\text{c}}^{'}}\frac{E_{\text{L}}}{f_{\text{c}}^{'}}} \tag{3}$$

In Eqn.(3), the presence of the McCauley bracket is because of the variation of the plastic dilation rate for high strength concrete. To implement the plastic dilation rate formulation in

the flow rule, a method involving the plastic dilation rate control parameter (α_{P0}) in the flow rule is used in [2]. Further a scaling function is introduced for the smooth transition of the plastic dilation rate from the beginning of plastic flow up to the peak stress. At the start of plastic flow, the plastic dilation rate is equal to zero and at the peak stress, the plastic dilation rate is equal to Eqn.(1).

In Figure 1, there are two regions of the plastic dilation rate. The first region is where the increment of the plastic volumetric strain is in compaction ($|\beta| < 0.5$) and the second region is where the increment of the plastic volumetric strain is in dilation ($|\beta| > 0.5$). The predicted plastic dilation rates in Figure 1 are generated using the expression from Eqn. (1). The predictions represent different stiffness of the external confining devices and their effect on the plastic dilation rate behavior of FRP confined concrete. Note that the observed value of the plastic dilation rate, which is shown in Figure 1, shows the peak plastic dilation rate. For actively confined concrete (E_L = 0 MPa), the plastic dilation rate asymptotes to a value of -0.5. As the E_L increases, the plastic dilation rate shifts to the plastic volumetric compaction region. This phenomenon occurs for FRP confined concrete with sufficiently high stiffness [6, 7].

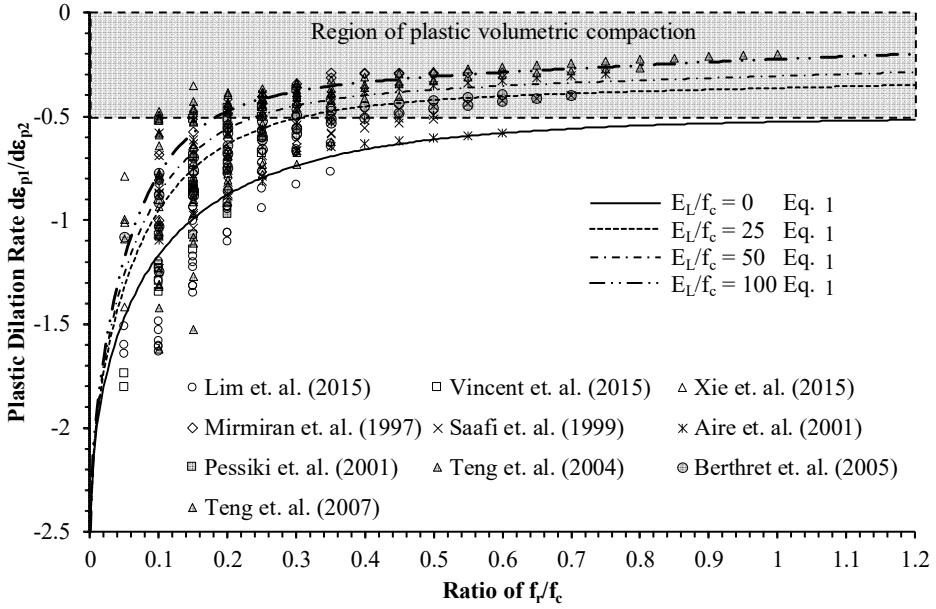

Figure 1 Plastic dilation rate behavior for FRP confined concrete [2]

Figure 2 shows the development of the plastic dilation rate for FRP confined concrete with different ply tested by [8] with ID 01-09. In Figure 2, the prediction of the plastic dilation rate using Eqn.(1) and also using the complete stress-strain curve for FRP confined concrete via the constitutive driver are presented. By looking at the complete development of the plastic dilation rate from the analysis, at the initial plastic flow, the value of the plastic dilation rate starts from zero and goes up to a value of -0.5. this region is called the initial plastic compaction. It is also worth mentioning that a flow rule that always dilates such as in [9, 10], will never be able to capture initial plastic compaction. After passing the initial plastic compaction region, the plastic dilation rate keeps increasing until reaching the peak plastic dilation ratio and continues to

follow the path of the peak plastic dilation rate as shown in Figure 2. Note, in the experiments, the plastic dilation rate also starts from zero. In Figure 2, however, the experimental plastic dilation rate is plotted once the minimum secant dilation rate is found in the experiment (see [2]) and therefore the plastic dilation rate from the zero point up to the minimum plastic dilation rate is not shown.

For CFST, it is expected that the plastic dilation rate after the steel tube yields should be almost equal to that of actively confined concrete ($E_L = 0$). After the steel yields, the confining pressure increases, the value for the initial lateral modulus will be small. The experiments carried out in [11] are examined and are used in this study. The work in [11] provides a complete data set which can be used for evaluating the plastic dilation rate for CFST. The axial stress in the concrete and the confining pressure is extracted, and Hook's law is used to compute the axial and lateral elastic strains. The axial and lateral plastic strains are further computed by subtracting the elastic strains from the total strains. The plastic dilation rate is obtained by computing the ratio of the lateral to axial plastic strains.

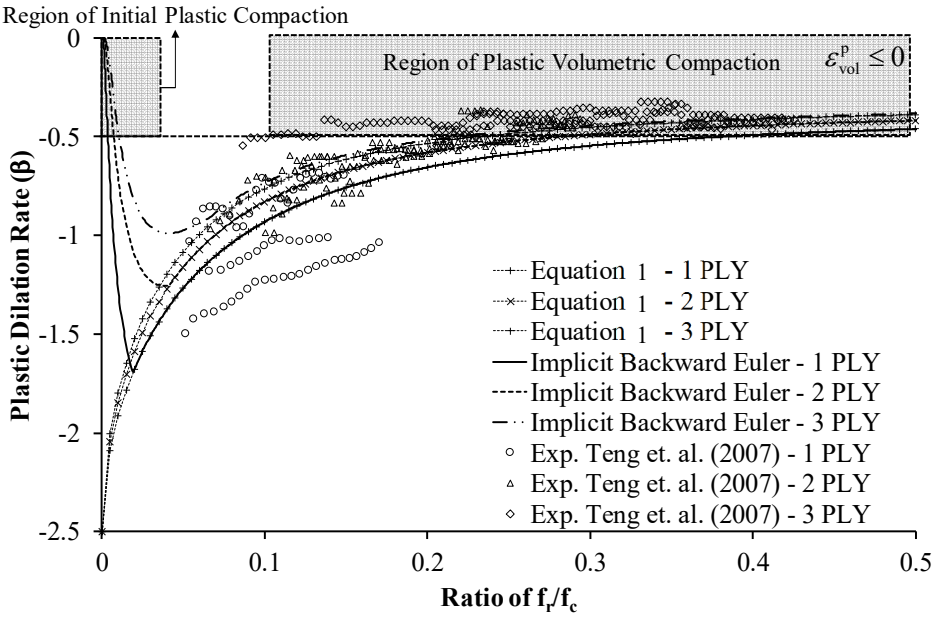

Figure 2 Comparison of the plastic dilation rate formulation with the constitutive driver and the experiments [2]

Figure 3 shows the plastic dilation rate behavior for CFST specimens taken from [11] are selected for investigation. Two specimens with normal strength concrete (NSC) and one specimen with high strength concrete (HSC) are selected. In Figure 3, the plastic dilation rates are plotted as a function of axial strain. In Figure 3, the peak plastic dilation rate are generated using Eqn. (1) with two different values of the lateral modulus. One with zero lateral modulus, which in Figure 3 is represented as the active model and the other with the lateral modulus calculated from the experiments and is represented as the passive model. Note, for zero confining pressure (uniaxial case) or when the confining pressure is tensile, the plastic dilation rate at the peak stress is equal to β_0 which is equal to -2.5. Hence, in Figure 3, at the initial loading stage, where the confining pressure is in tension (see [11]), the peak plastic dilation rate is equal to -2.5.

The plastic dilation rate from all the specimens starts at zero plastic dilation rate which clearly identifies the initial plastic volumetric compaction for CFST specimens. As the loading increases, the absolute value of the plastic dilation rate also increases up to the maximum value. For NSC, it is difficult to distinguish between the maximum and the minimum values of the plastic dilation rate once the steel tube yields. However, for the HSC specimen, we can easily distinguish between the maximum and the minimum values of the plastic dilation rate. The maximum absolute plastic dilation rate for the 80 MPa concrete occurs at an axial strain of about -0.0025 and as the loading increases, the plastic dilation rate drops to a value of -1.2. Notice that there is a small increase in the plastic dilation rate throughout the loading for HSC while for NSC, the plastic dilation rate is almost constant.

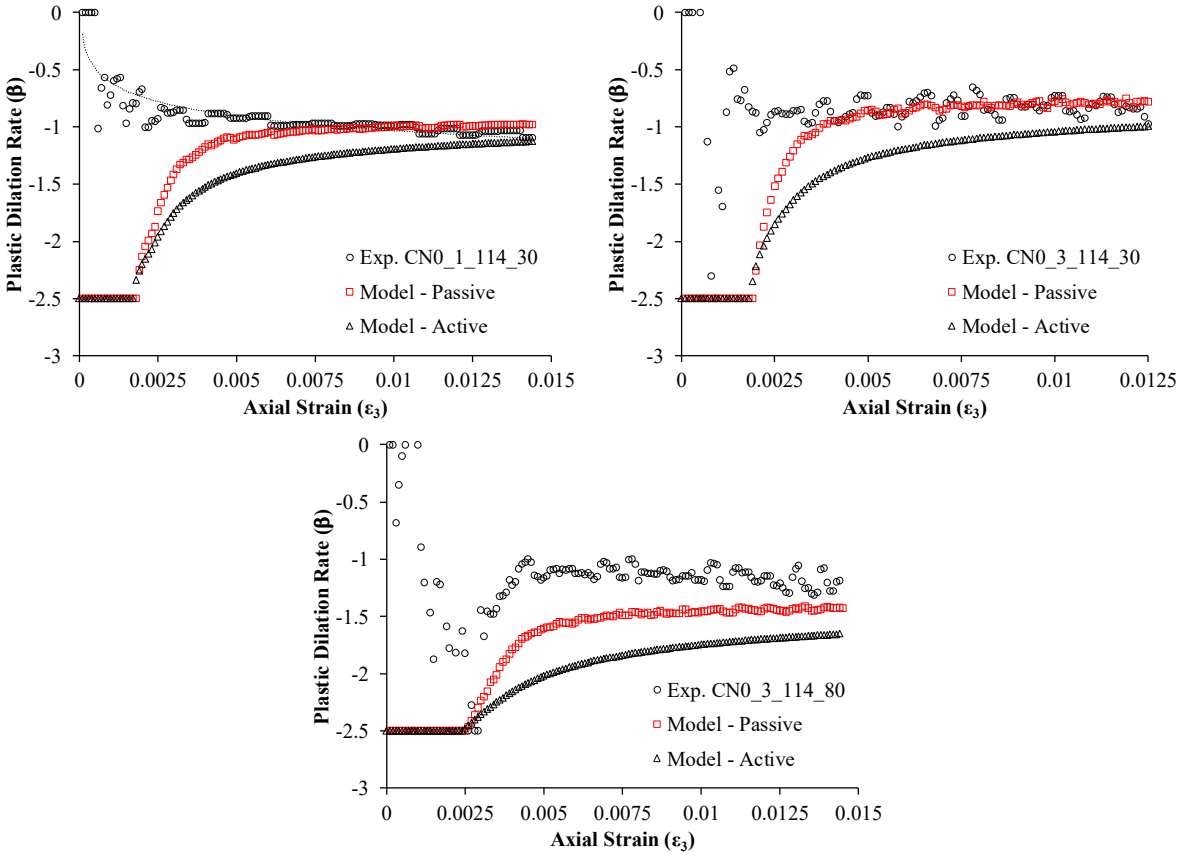

Figure 3 Plastic dilation rate behavior for CFST specimens

For normal strength concrete, the prediction of the plastic dilation rate for CFST is excellent. The model for passively confined concrete can capture the plastic dilation rate behavior of CFST while the actively confined concrete model has a higher plastic dilation rate. From both the experiments and the model prediction, the plastic dilation rate is almost constant after the CFST yields. However, the almost constant plastic dilation rate does not mean that the confining pressure is constant. The confining pressure is still increasing but the lateral modulus decreases which means the effectiveness of the external confining device is also decreasing. This finding is important and the model can explain this behavior clearly. A model without a clear definition between active and passive modes cannot identify this difference and although these models

may provide good predictions, they lack the explanation of what is happening in the experiments.

For high strength concrete, the prediction of the plastic dilation rate is lower in absolute terms than the experiments. When evaluating the experimental data for FRP confined concrete, there is a term inside the McCauley bracket Eqn.(3) to cater for the test results available for HSC which were from one source and had a compressive strength of 73 MPa. The term has a purpose to accelerate the increase in the plastic dilation rate for high strength concrete. It is therefore important to investigate more HSC experimental results and re-evaluate Eqn.(3). Further, for a CFST specimen, the yielding of the steel tube lowered the value of the lateral modulus, and thus the limit of plastic dilation rate as shown in Eqn.(2) remain untouched.

3 MODELLING AND DISCUSSION

This section presents two finite element models for CFST short column specimen using an in-house three-dimensional non-linear finite element analysis (3DNLFEA) program. 3DNLFEA is an in-house program developed by the authors which focuses on non-linear analysis for reinforced concrete structures. 3DNLFEA is now under heavy development focusing on parallel computation and the use of Graphical Processing Unit (GPU) to improve the computational performance. The pre- and post-processor use SALOME [12] and ParaView [13, 14], respectively. In solving the global equilibrium equations in the non-linear finite element analysis, the initial elastic stiffness method combined with a process modification [15] (acceleration technique) are used in the analysis. The constitutive model for concrete and steel materials are based on the plasticity model developed by the authors [2, 3] and a J2 plasticity with zero hardening modulus, respectively. The 2nd order effects are considered using an updated Lagrangian formulation.

Two experiments from Lai and Ho [11] are selected for comparisons. The first and the second specimen have an annotation of CN0_4_139_100 and CN0_8_168_120, respectively. The first term of the annotation which is "CN0" shows that the specimen is a pure CFST column with no additional external confining devices provided. The second term shows the thickness of the steel tube in mm. The outer diameter (mm) is shown in the third term and the uniaxial concrete compressive strength (MPa) is shown in the fourth term. The height of the CN0_4_139_100 and CN0_8_168_120 specimens are 420 mm and 330 mm, respectively. The CN0_4_139_100 and CN0_8_168_120 specimens are constructed with 1,953 and 1,944 hexahedral elements, respectively. Both ends of the CFST column are fixed. The loading in the analysis is controlled using a displacement control applied at the top end of the specimen.

Figure 4 and Figure 5 shows the meshed elements, Von-Mises stresses, the hardening parameter and the lateral modulus for the CN0_4_139_100 and CN0_8_168_120 specimens, respectively. The output data was evaluated at the final load step. The Von-Mises stress distribution in concrete for both specimens is similar despite the different ratio of the height over diameter (l/d) of the specimen (see Figures 1b and 2b). Since both ends of the specimens were fixed, the localization during softening occurs at the mid-height of the specimen. From Figures 4c and 5c, the hardening parameter (k), which is a measure of cumulative plastic volumetric strain, has the highest value at the mid height. As for the lateral modulus, theoretically, if there are no increases in the confining pressure, the value of the lateral modulus should be zero. However, the values of the lateral modulus shown in Figures 4d and 5d are not

zero which explains that even under softening, the confining pressure is still increasing.

Figure 6 and Figure 7 show the comparison of the axial force versus the axial strain between the 3DNLFEA and the experimental results. Note that in Figures 6 and 7, the input data for the 3DNLFEA is shown below the specimen ID. For example, in Figure 6, the first line below the specimen ID identifies the actual concrete compressive strength in MPa (F104.5), the Young's Modulus of the concrete in GPa (E34.5) and the concrete uniaxial axial peak strain at the peak stress (EPS0.0038). The second line below the specimen ID shows the actual yield stress of the steel tube in MPa (S361), the Poisson's ratio of the steel tube (P0.29), the Young's Modulus of the steel tube in GPa (E205) and the thickness of the steel tube in mm (T7.82).

From the comparisons, the overall predicted responses for both specimens are in good agreement. The prediction of the peak axial load for CN0_4_139_100 is slightly higher than the experiment and the traced softening response is steeper than the experiment. However, the predicted residual stress, where the axial load is almost like a plateau, is in good agreement with the experiments. For the CN0_8_168_120 specimen, the predicted peak stress and peak strain are excellent. The softening response is excellent up to some degree, however, as the specimen softens further, the predicted axial load carrying capacity is higher than the experiment.

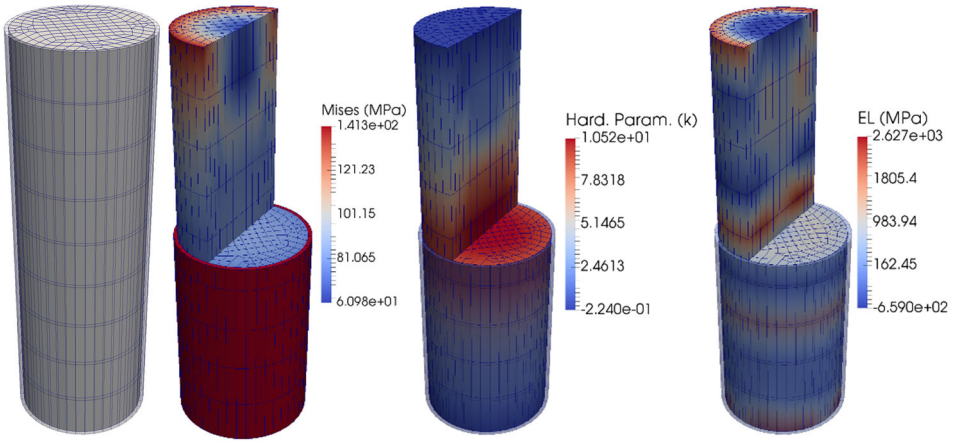

(a) (b) (c) (d)

Figure 4 (a) 3D Model of CN0_4_139_100 specimen (b) Von-Mises Stress (c) Hardening parameter (d) Lateral Modulus parameter (E_L)

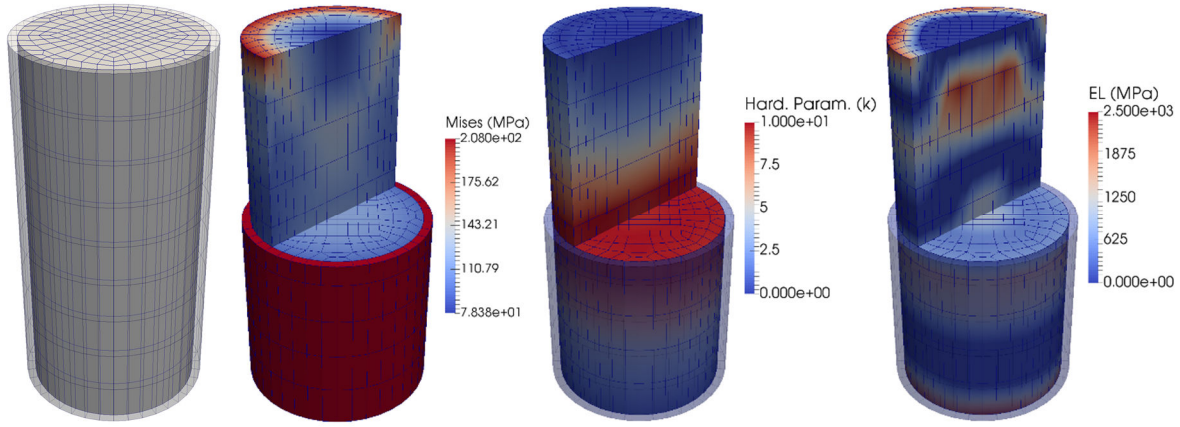

(a) (b) (c) (d)

Figure 5 (a) 3D Model of CN0_8_168_120 specimen (b) Von-Mises Stress (c) Hardening parameter (d) Lateral Modulus parameter (E_L)

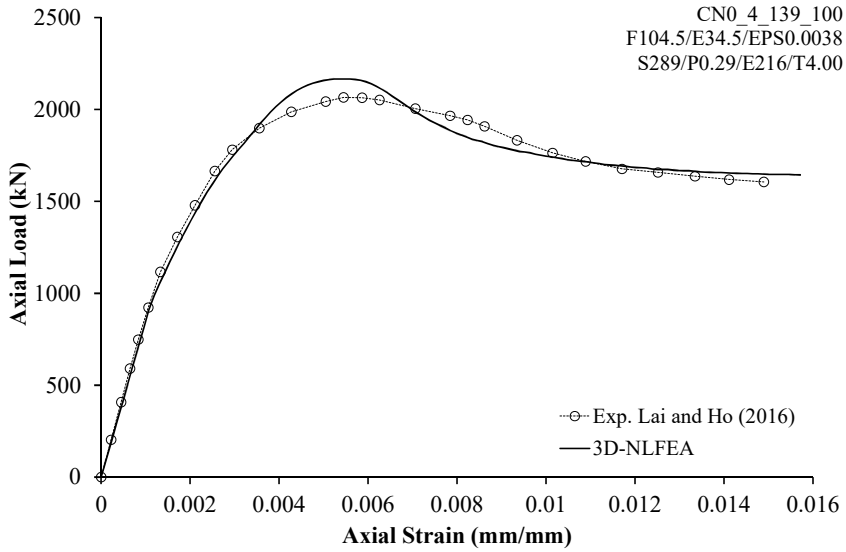

Figure 6 Comparison between 3DNLFEA and CN0_4_139_100 experimental result

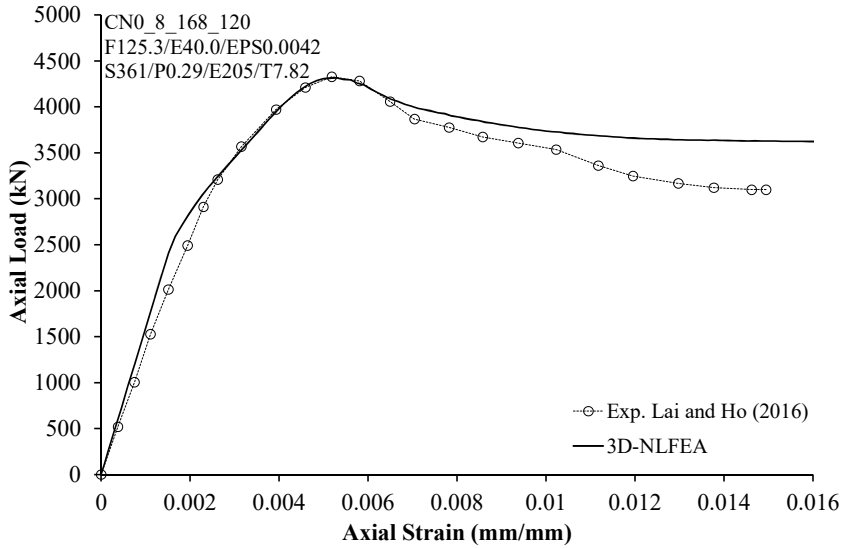

Figure 7 Comparison between 3DNLFEA and CN0_8_168_120 experimental result

4 CONCLUSIONS

This paper investigates the plastic dilation rate behavior of CFST columns. The experimentally extracted plastic dilation rates are compared with the plastic dilation rate formulation proposed by the authors. The comparison of the plastic dilation rate shows good agreement despite slightly higher prediction for high strength concrete. For a concrete-filled-steel-tube (CFST) specimen, once the steel tube yields, the value of the lateral modulus drops and thus the limit of the plastic dilation rate [2] remains untouched. Further, it was found that for normal strength concrete, the plastic dilation rate after the steel tube yields is almost constant. However, this did not mean that the confining pressure is constant. The confining pressure increases, but the lateral modulus reduces and produces an almost constant plastic dilation rate. Although the plastic dilation formulation was initially developed using data from FRP confined concrete, the formulation is also valid for CFST specimens. To further verify the developed plasticity constitutive model, comparisons between the CFST experiments from the literature with the non-linear finite element analysis (3D-NLFEA) were also presented. The comparisons between the model and the experiments were excellent with sufficiently high accuracy prediction of the peak axial load and peak axial strain. Further work will concentrate on obtaining more experimental data for high strength concretes.

REFERENCES

[1] S. Pantazopoulou, "Role of expansion on mechanical behavior of concrete," *Journal of structural engineering,* vol. 121, pp. 1795-1805, 1995.

[2] B. Piscesa, M. M. Attard, and A. K. Samani, "A lateral strain plasticity model for FRP confined concrete," *Composite Structures,* vol. 158, pp. 160-174, 2016.

[3] B. Piscesa, M. Attard, A. Samani, and S. Tangaramvong, "Plasticity Constitutive Model for Stress-Strain Relationship of Confined Concrete," *ACI Structural Journal,* vol. 114, p. 361, 2017.

[4] B. Piscesa, M. M. Attard, and A. K. Samani, "Three-dimensional Finite Element Analysis of Circular Reinforced Concrete Column Confined with FRP using Plasticity Model," *Procedia Engineering,* vol. 171, pp. 847-856, 2017.
[5] A. K. Samani and M. M. Attard, "Lateral Strain Model for Concrete under Compression," *ACI Structural Journal,* vol. 111, 2014.
[6] A. Mirmiran and M. Shahawy, "Dilation characteristics of confined concrete," *Mechanics of Cohesive-frictional Materials,* vol. 2, pp. 237-249, 1997.
[7] S. Tastani, I. Balafas, A. Dervisis, and S. Pantazopoulou, "Effect of core compaction on deformation capacity of FRP-jacketed concrete columns," *Construction and Building Materials,* vol. 47, pp. 1078-1092, 2013.
[8] T. Jiang and J. Teng, "Analysis-oriented stress–strain models for FRP–confined concrete," *Engineering Structures,* vol. 29, pp. 2968-2986, 2007.
[9] V. K. Papanikolaou and A. J. Kappos, "Confinement-sensitive plasticity constitutive model for concrete in triaxial compression," *International Journal of Solids and Structures,* vol. 44, pp. 7021-7048, 2007.
[10] J. Bao, X. Long, K. H. Tan, and C. K. Lee, "A new generalized Drucker–Prager flow rule for concrete under compression," *Engineering Structures,* vol. 56, pp. 2076-2082, 2013.
[11] M. Lai and J. Ho, "A theoretical axial stress-strain model for circular concrete-filled-steel-tube columns," *Engineering Structures,* vol. 125, pp. 124-143, 2016.
[12] CEA/DEN, EDF_R&D, and OPEN_CASCADE, "SALOME - The Open Source Integration Platform for Numerical Simulation. http://www.salome-platform.org/," Ver. 7.8.0 ed, 2016.
[13] J. Ahrens, B. Geveci, C. Law, C. Hansen, and C. Johnson, "36-ParaView: An End-User Tool for Large-Data Visualization," *The Visualization Handbook,* p. 717, 2005.
[14] U. Ayachit, "The paraview guide: a parallel visualization application," 2015.
[15] R. Lawther, "Modification of iterative processes for improved convergence characteristics," *International Journal for Numerical Methods in Engineering,* vol. 15, pp. 1149-1159, 1980.